ELSEVIER

Sensors and Actuators A 91 (2001) 326–332

SENSORS AND ACTUATORS A PHYSICAL

www.elsevier.nl/locate/sna

Active frequency tuning for micro resonators by localized thermal stressing effects☆

Todd Remtema[1], Liwei Lin*

Department of Mechanical Engineering, University of California, 5126 Etcheverry Hall, MC 1740, Berkeley, CA 94720-1740, USA

Abstract

A method of active frequency tuning on comb-shape micro resonators has been successfully demonstrated by means of localized stressing effects. A mechanical beam structure that can be resistively heated to generate thermal stress, is integrated as part of the comb-shape micro resonator for frequency tuning. Experimentally, a frequency change up to 6.5% is measured for resonators with a central frequency at around 31 kHz. The required tuning power is 25 mW in the form of localized Joule heating. Analytically, both a one-dimensional electrothermal model and a dynamic model are established to characterize the electrical, thermal and frequency responses of active frequency tuning. The simulation results of frequency spectrum are consistent with experimental measurements. A reliability test, conducted for more than 300 million cycles under 6.5% of frequency tuning range, reveals no observable material damages on the micro resonator. This scheme enables active frequency tuning under low power consumption and independent of the input/output function of a micro resonator. As such, it has potential applications to resonator-based MEMS devices, such as rate gyroscopes and microelectromechanical filters.

Keywords: Electrothermal; Resonator; Joule heating

1. Introduction

Micro resonators have been used in various resonator-based microsystems, such as resonant accelerometers [1,2], microelectromechanical filters [3–5], and gyroscopes [6,7]. One common roadblock in the manufacturing process comes from local process variations. As a result, even though the micro fabrication process is well controlled, structural deviations exist between designed and fabricated devices and between same devices adjacent to each other on the same wafer. Therefore, it is common that the frequency responses of micro resonators may be off from the desired design value and should be eradicated by post-tuning processes. For example, the resonant frequency in the widely used comb-shape micro resonator can vary a few percentages on the same chip [8].

Frequency tuning methods can be split into two major categories, those that make one-time permanent changes and those that make active adjustments without permanent damages to microstructures. The permanent changes can be accomplished by annealing the folded springs of a comb-structure using voltage pulses to change the stiffness and quality factor [9] or by a post-deposition process [10]. On the active frequency tuning side, three basic methods have been investigated. The first of these is tuning via an ''electrostatic stiffness'' change, where the stiffness can be adjusted electrostatically with capacitive structures [6,11–14]. The second method tunes by making changes in the internal stresses of the structure to induce changes in resonance [15–18]. The third method takes advantage of the inherent temperature dependence of Young's modulus [19].

The method presented in this work takes advantage of the temperature dependence of Young's modulus exhibited by most materials as well as the thermally induced internal stress effects. That is, as the temperature of polysilicon goes up, its Young's modulus drops and this will cause a minor reduction in the resonant frequency. The localized thermal stress generated by Joule heating plays a major role in the proposed frequency tuning scheme. If a compressive stress is generated, the structure becomes more compliant resulting in a lower resonant frequency. If a tensile stress is generated, the structure becomes stiffer resulting in a higher resonant frequency. Through the use of filament-like heating as implemented in this work, the device heats up resulting

☆A portion of this paper is presented at the Transducers Research Founation Hilton Head Workshop on Solid-State Sensor and Actuators, Hilton Head, SC, 2000.

* Corresponding author. Tel.: +1-510-643-5495; fax: +1-510-643-5599.
E-mail address: lwlin@me.berkeley.edu (L. Lin).

[1] Present address: Mechanical Engineering and Applied Mechanics Department, University of Michigan, Ann Arbor, MI, USA.

0924-4247/01/$ – see front matter
PII: S0924-4247(01)00603-3

in a decrease in Young's modulus and an increase in compressive stresses. Both effects help to actively lower the resonant frequency.

2. A tunable micro resonator

A tunable micro resonator by means of localized thermal stressing effects has been designed as illustrated in Fig. 1. The comb-drive structure is modified by replacing one folded-beam suspension with a straight suspension as the tuning beam. The folded-beam suspension helps minimizing the non-linear effect that may arise from the straight-beam structure design [20,21]. One drawback of this folded-beam/straight-beam design as opposed to a straight-beam/straight-beam design is that the tuning range of the device is reduced. However, most non-linear effects are avoided by the current design. The straight-beam suspension is 4 μm wide and 165 μm long. On the folded-beam suspension, the four beams are 2 μm wide and 150 μm long and the truss is 5 μm wide and 36 μm long. The anchors on the two sides of the suspension system are electrically isolated such that a voltage can be applied across the structure. This voltage heats the structure through filament-like heating that causes the structure itself to heat up and to expand. During the heating process, the substrate stays relatively cool due to the rapid heat transfer capabilities of silicon.

A standard surface-micromachining process provided by MCNC [22] is used to fabricate these tunable micro resonators and all the simulation and experimental measurements presented here are based on the MUMPS-22 run. A sheet resistance of 6.4 Ω/sq and a thermal coefficient of resistivity of 1.7×10^{-3} Ω/K are measured for the structural polysilicon layer. Young's modulus and density of the polysilicon layer used in this work are 160 GPa and 2300 kg/m^3. The thermal coefficient of expansion and specific heat of polysilicon are adopted from silicon as 2.6×10^{-6}/K and 712 J/kg K, respectively. The values of thermal conductivity of the silicon, polysilicon, and nitride layers used in this paper are 148, 34, and 1.6 W/m K.

The frequency responses of the device are measured using a CCD camera built into a probe station. Pictures are first taken and then opened in Canvas™ [23] and the amplitudes of vibration for every 100 Hz of driving frequency are measured and recorded. Measurements of resonance are obtained by adjusting the driving frequency until the peak driving amplitude of the device could be observed. This method could locate the resonant frequency within 100 Hz when the resonant frequency is typically around 30 kHz. This gives an accuracy of roughly 0.33%.

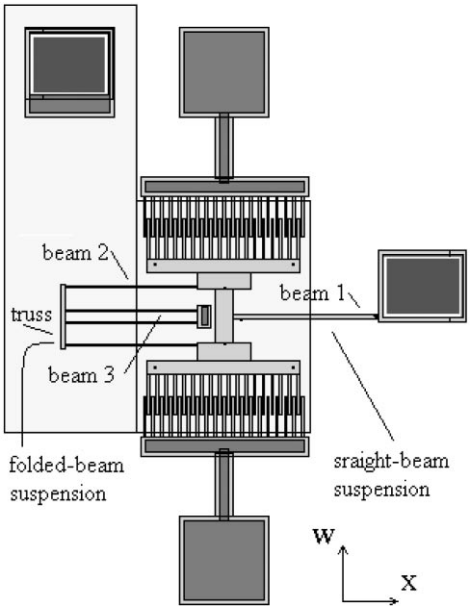

Fig. 1. Schematic diagram of a comb-shape micro resonator with a straight-beam for active frequency tuning via localized stressing effects.

3. Dynamic and electrothermal model

3.1. Dynamic model

A simplified dynamic model is illustrated in Fig. 2, where K_x is the stiffness of the truss of the folded-beam suspension in the x direction and k the stiffness of the folded-beam suspension in the w direction. The straight-beam suspension has the moment of inertia, I, cross-sectional area, A, and length L. The Young's modulus and density of the structural material are represented as E and ρ, respectively. M_{eff} is the effective mass of the combination of the folded-beam suspension and the rigid central portion of the device. The equations of motion governing the transverse vibration $w(x,t)$ as a function of the position x along the length of the beam and the time t is given by the following linear partial differential equation:

$$EI\frac{\partial^4 w}{\partial x^4} + P\frac{\partial^2 w}{\partial x^2} + \rho A\frac{\partial^2 w}{\partial t^2} = -q(x) \tag{1}$$

P can be given by the following equation:

$$P = K_x(\Delta L_1 + \Delta L_2 + \Delta W - \Delta L_3) \tag{2}$$

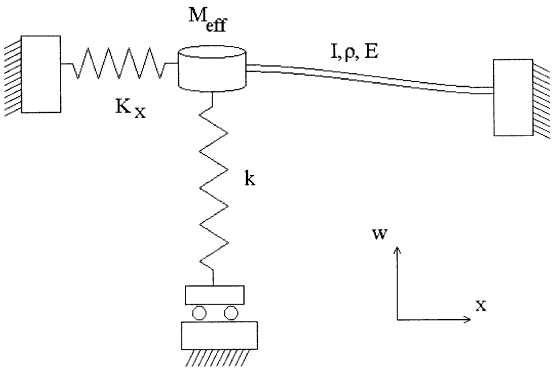

Fig. 2. A simplified dynamic model.

where ΔL_1, ΔL_2, and ΔL_3 are the changes in length of beams 1, 2, and 3 and ΔW the change in width of the central mass as illustrated in Fig. 1 due to resistive heating. The goal of this model is to predict the resonant frequency given a certain force P. This can be done by setting $q(x) = 0$ and by using separation of variables, i.e. setting $w(x,t)$ equal to $X(x)T(t)$, where $T(t) = C\sin(\omega t + \theta)$. Given that C and θ are constants, $w(x,t) = X(x)T(t)$ and $q(x) = 0$ can be substituted into Eq. (1) to give the following equation:

$$\omega^2 = \frac{EI}{\rho A}\frac{1}{X}\frac{\mathrm{d}^4X}{\mathrm{d}x^4} + \frac{P}{\rho A}\frac{1}{X}\frac{\mathrm{d}^2X}{\mathrm{d}x^2} \tag{3}$$

The general solution for $X(x)$ can be given by

$$X(x) = C_1\sinh\left(\frac{ax}{L}\right) + C_2\cosh\left(\frac{ax}{L}\right) + C_3\sin\left(\frac{bx}{L}\right) + C_4\cos\left(\frac{bx}{L}\right) \tag{4}$$

where C_1, C_2, C_3, and C_4 are unknown constants and

$$a^2 = -\frac{PL^2}{2EI} + \sqrt{\left(\frac{PL^2}{2EI}\right)^2 + \omega^2\frac{\rho AL^4}{EI}} \tag{5}$$

$$b^2 = \frac{PL^2}{2EI} + \sqrt{\left(\frac{PL^2}{2EI}\right)^2 + \omega^2\frac{\rho AL^4}{EI}} \tag{6}$$

The following boundary conditions are used:

$$X|_{x=0} = 0 \tag{7}$$

$$\left.\frac{\mathrm{d}X}{\mathrm{d}x}\right|_{x=0} = 0 \tag{8}$$

$$\left.\frac{\mathrm{d}X}{\mathrm{d}x}\right|_{x=L} = 0 \tag{9}$$

$$(k - \omega^2 M_{\mathrm{eff}})X - EI\left.\frac{\mathrm{d}^3X}{\mathrm{d}x^3}\right|_{x=L} = 0 \tag{10}$$

A symbolic solution for ω is not possible such that a numeric solution is implemented to find solutions for ω.

3.2. Electrothermal model

In the previous section, a dynamic model is developed which predicts the resonant frequency given a force P. This force was given as a function of the change in length of each of the supporting beams and the change in width of the rigid central portion of the device. This change in length and width comes from the thermal expansion of polysilicon when heated. In order to make an accurate prediction of the changes in dimensions of the device, a thermal analysis is developed based on a one-dimensional discrete time and space model. The moving comb-drive is first split into smaller thermal masses. The straight-beam suspension is split into 40 pieces, the folded-beam suspension is split into 58 pieces, and the central rigid portion is split into 2 large masses. Each of these masses are treated as shown in Fig. 3, where T_i is the temperature of the ith node and $T_{\mathrm{substrate}}$ is the temperature of the substrate which is assumed to remain constant at room temperature. $I^2R(T)$ is the power going into the ith node where I is the current flowing through the node and R the electrical resistance of the node. The resistance is temperature-dependent and can be expressed by the following equation:

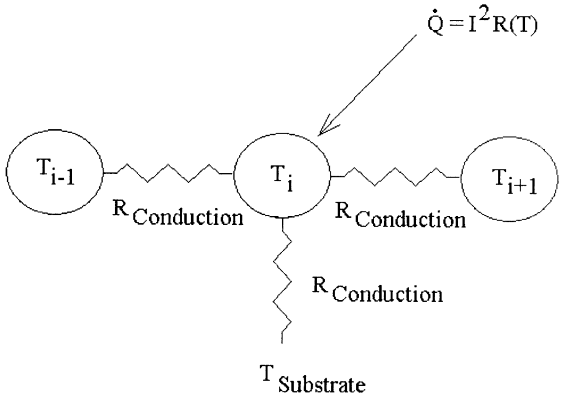

Fig. 3. A nodal point illustrating the electrothermal model.

$$R(T) = R_0[1 + 1.7E^{-3}(T - T_0)] \tag{11}$$

where R_0 is the resistance at a temperature T_0. Heat is dissipated away from the ith thermal mass via convection, radiation, and conduction. The first two of these mechanisms, convection and radiation, are considered negligible compared to conduction and are neglected [24]. Conduction happens between the ith node and its adjacent nodes and can be expressed by the following equation:

$$Q_{\mathrm{conduction}} = \frac{k_{\mathrm{po}}A}{x}(T_i - T_{i\pm1})\Delta t \tag{12}$$

where k_{po} is the thermal conductivity of polysilicon, x the distance between centers of adjacent nodes, $T_{i\pm1}$ the temperature of the adjacent node and Δt the time period. Heat also conducts into the substrate by the following equation:

$$Q_{\mathrm{substrate}} = \frac{1}{R_{\mathrm{eff}}}(T - T_{\mathrm{substrate}})\Delta t \tag{13}$$

where R_{eff} is the effective thermal resistance of the air, polysilicon layer, and nitride layers and is given by

$$R_{\mathrm{eff}} = \frac{1}{F_sA_b}\left(\frac{h_{\mathrm{air}}}{k_{\mathrm{air}}} + \frac{h_{\mathrm{po}}}{k_{\mathrm{po}}} + \frac{h_{\mathrm{ni}}}{k_{\mathrm{ni}}}\right) \tag{14}$$

where k_{air} is the thermal conductivity of air, k_{ni} the thermal conductivity of the nitride layer, A_b the area of the bottom surface of the thermal mass, h_{air} the suspension distance of the beam to the substrate, h_{po} the thickness of the ground polysilicon layer, and h_{ni} the thickness of the nitride layer. F_s is a heat conduction shape factor to take into account the spreading of heat into the substrate [25]. The simulated shape factor for beam widths of 2 and 4 μm are 4.07 and 2.92, respectively.

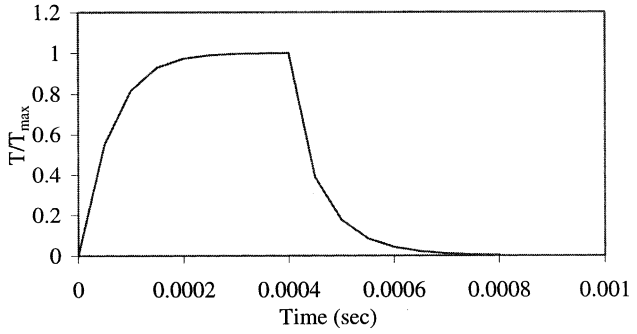

Fig. 4. Transient temperature simulation.

With this model, the change in temperature over a small period of time Δt can be accurately predicted using the following equation:

$$\Delta T = \frac{I^2 R(T)\Delta t - Q_{\text{conduction}} - Q_{\text{substrate}}}{C_{\text{p}} m} \tag{15}$$

where C_{p} is the specific heat of polysilicon and m the mass of the ith node. With this change in temperature, the ith node can then be assigned a new temperature and Eq. (15) can be used again to find the change in temperature for the next Δt continuously until the temperature reaches a steady state.

With this model, the transient responses of the temperature versus time can be graphed as seen in Fig. 4. The rising and falling times for the system to reach steady state under heating and cooling are found to be around 140 μs. Using the model developed above, a temperature profile of the system at a time significantly larger than the rise time can be attained as shown in Fig. 5. Nodes 1–25 are the inner portion of the folded-beam suspension, nodes 26–32 are the truss portion of the folded-beam suspension, nodes 33–58 are the outer portion of the folded-beam suspension, node 59 and 60 are the rigid central mass, and nodes 61–100 are the straight-beam suspension. Fig. 6 is an optical photo showing the tunable micro resonator under a microscope. When a high tuning power is supplied for resistive heating of the system and the background light is turned off, Fig. 7 shows the hot spots. When Fig. 7 is compared with Fig. 5, the highest temperature region agrees well with what is seen experimentally. The temperature simulations under various input power are used to predict the thermal expansion of comb-drive to derive the tuning force P and frequency changes.

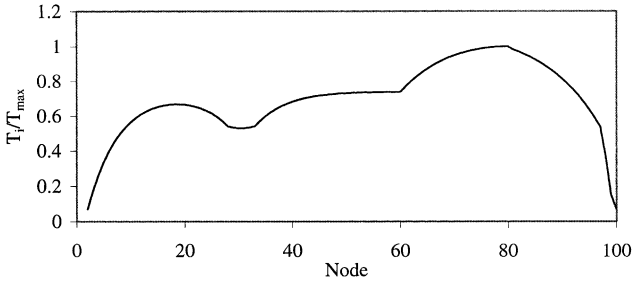

Fig. 5. Temperature profile simulated by the electro-thermal model.

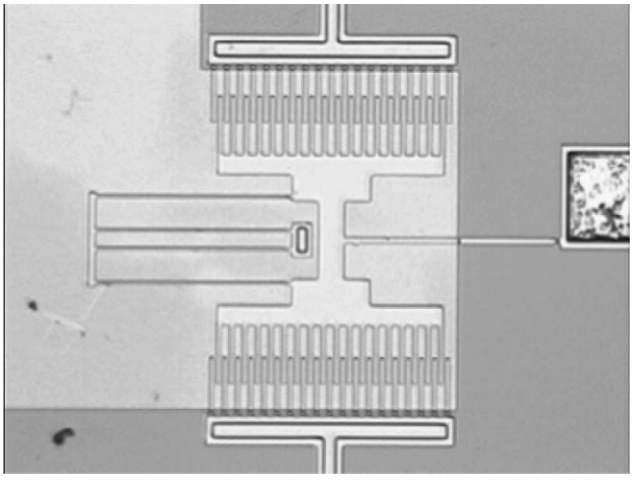

Fig. 6. A tunable resonator under an optical microscope.

Fig. 7. Hot spots are shown under the Joule heating effects when the light on the optical microscope is turned off.

4. Experimental results and discusions

Using the experimental set-up described earlier, four basic tests have been conducted on the tunable resonator. The first test is a comparative test where the resonator is heated by external means and by localized Joule heating, respectively. The external heating is accomplished by placing the device on a hot plate. In both tests, the resistance of the suspended beams is measured at various temperatures when resonant frequency change is measured. The resistance is used as the guidance to estimate the temperature of the device. Fig. 8 shows the resonant frequency changes with respect to the resistance changes (temperature changes). It is found that when the resistance is at 940 Ω it corresponds to an average temperature of 150°C. At this temperature, the external heating causes a frequency change of about 1% and the

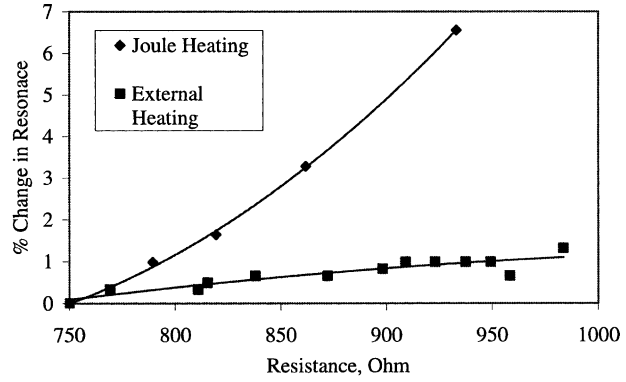

Fig. 8. Frequency changes by means of external (global) heating and Joule (localized) heating.

internal Joule heating makes the frequency change of 6.5%. Under this Joule heating condition, the maximum temperature at the tuning beam is 255°C and the average temperature of the resonator is 150°C. It is concluded that under the same average temperature, the Joule heating causes the resonance to change much more than the external heating. The external heating makes both the substrate and the device to expand such that this keeps the thermal stressing effects to a minimum. The change in resonance by external heating can be attributed mainly to the change in Young's modulus and partially to the change in density and thermal mismatch. The temperature coefficient of Young's modulus can be found using the following equation [3]:

$$TC_f = \frac{1}{2}(TC_E - TC_h) \quad (16)$$

where TC_f is the temperature coefficient of the resonant frequency, TC_E the temperature coefficient of Young's modulus and TC_h the temperature coefficient of thermal expansion. In this work, TC_E is found to be -40 ppm/°C by the external heating experiments, and the magnitude is close to previously reported values [3–5]. In the Joule heating case, the device itself heats up where as the substrate stays relatively cool. This creates a large internal stressing effect as well as a change in Young's modulus.

The second experiment is to check for repeatability and compliance of the dynamic and electrothermal models. In this test, five different structures from four different dice are tested over a range of tuning powers. The change in resonance verses the applied tuning power is plotted for five different devices along with the predicted theoretical response as shown in Fig. 9. As seen in the plot, the theory predicts a quasi-linear change in resonance versus input power. The experimental data points are close to the theoretical prediction when the input power is lower than 30 mW. However, the model is only valid for a first-order approximation because it does not take into account several secondary effects, including non-linearity due to the softening of the spring as the structure deflects, the change in specific heat, thermal conductivity, and the thermal coefficient of expansion as the temperature increases. When the input power is higher than 30 mW, the frequency responses deviate from the analytical prediction. Moreover, permanent damages are observed to the micro resonators such that they are not able to return to the original resonant frequency after the tuning power is turned off. Although, further research is required to investigate the structural changes with respect to temperature and stress levels, it is believed that polysilicon creep [26] may have played an important role.

The third test is to measure the spectrum response of the resonator. One device is tested in this manner. The driving frequency is changed every 100 Hz and the amplitude is recorded. This is done by scanning both into the higher frequencies and into the lower frequencies until the amplitude is relatively low. Several tuning currents are conducted and recorded as shown in Fig. 10 from 0 to 5 mA. As seen in the plot, the system starts out with a fairly linear response. As the tuning current is increased, the response begins to go more and more non-linear. This effect is to be expected. Non-linearity arises from the stiffening of the straight-beam suspension as the device deflects. The stiffening comes from the stretching of the beam as it deflects. This stretching increases the restoring force of the spring. It is well documented that as the magnitude of the intrinsic stress goes up

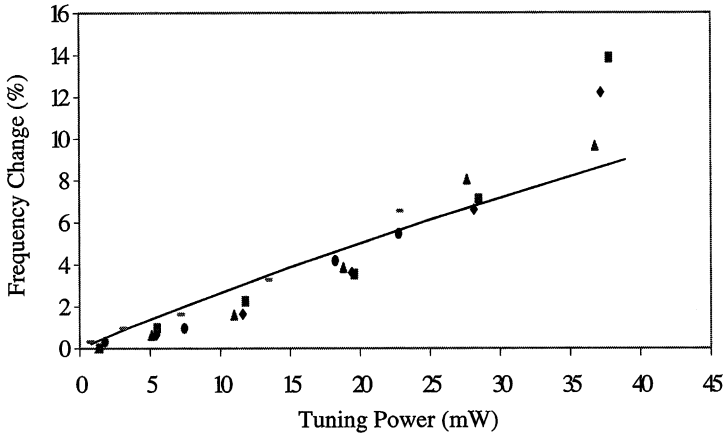

Fig. 9. Measured frequency changes vs. tuning power for five different devices compared to the theoretical model.

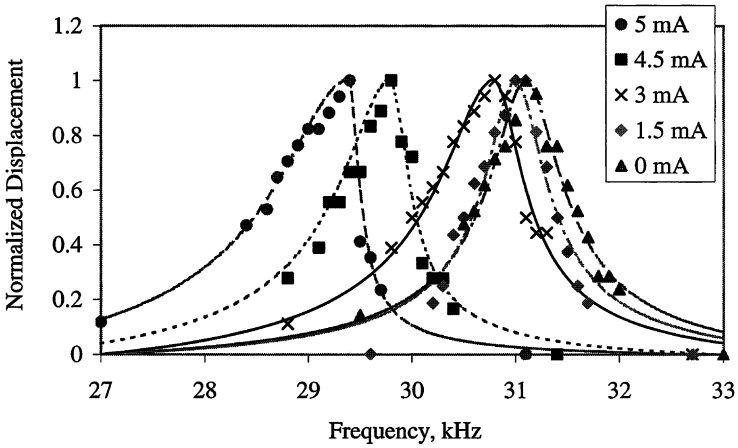

Fig. 10. Frequency spectrum of one device at five different tuning amperages from 0 to 5 mA.

the non-linearity also goes up [13]. Also seen in the plot is that the quality factor of the system stays nearly the same at about 50. This is because most of the dampening comes from the friction with the air that remains relatively unchanged during the frequency tuning process.

The final test is the reliability experiment for the tuning method. A resonator is tuned 1% and again to 6.5% for approximate 300 million cycles at 31 kHz, respectively. At the end of these tests, no visual damages can be found on the device. Most importantly, it returns completely to its original natural frequency and the measured resistance does not change before and after the tests. This indicates that there is no structural degradation and the active tuning method via thermal stressing effects as presented is feasible for repeated, long-term applications. Although, structural damage is not expected at the tuning power of 6.5% with a highest temperature at 255°C, further investigations should be conducted for the fatigue and creep [26] phenomena under high temperature and high stress operations.

5. Conclusion

An active frequency tuning mechanism has been proposed and has been proven to adjust the natural frequency of the comb-shape micro resonators up to 6.5% with minimal power requirements at 25 mW. This method can be applied at the component level after the completion of the packaging process and it can actively tune the frequency of micro resonators with a response time of 140 μs. It is important for microstructures to have frequency tuning capabilities in order to adjust for manufacturing variations in microsystems. Both dynamic and electrothermal models are established in this work to provide the design guidelines for active frequency tuning. Four different kinds of experiments have been conducted. The experiment of external versus Joule heating demonstrates that the thermal stressing effect is the dominant factor in the proposed tuning mechanism. The second experiment measured five different devices for frequency changes at various tuning powers. It is concluded that the analytical model is consistent with the experimental results. The third experiment measured the spectrum of comb-resonator at various tuning power. It is found that non-linear effects begin at high tuning power probably due to the spring stiffening effect. Finally, long-term tests for 300 million cycles demonstrate the good reliability of the presented tuning mechanism.

Acknowledgements

The authors would like to thank Mr. M. Chiao for discussions about the electrothermal model, Mr. J.-H. Tsai and Mr. B. Casey for wire bonding and packaging of the resonators. This work is supported in part by an NSF CAREER award (ECS-0096098) and a DARPA/MTO/MEMS grant (F30602-98-2-0227).

References

[1] T.A. Roessig, R.T. Howe, A.P. Pisano, J.H. Smith, Surface-micromachined resonant accelerometer, in: Proceedings of the International Conference on Solid-State Sensors and Actuators (Transducers 97), Chicago, 16–19 June 1997, pp. 859–862.
[2] Y. Omura, Y. Nonomura, O. Tabata, New resonant accelerometer based on rigidity change, in: Proceedings of the International Conference on Solid-State Sensors and Actuators (Transducers 97), Chicago, 16–19 June 1997, pp. 855–858.
[3] L. Lin, R.T. Howe, A.P. Pisano, Microelectromechanical filters for signal processing, J. Microelectromech. Syst. 7 (3) (1998) 286–294.
[4] K. Wang, C.T.-C. Nguyen, High-order micromechanical electronic filters, in: Proceedings of IEEE International Microelectromechanical Systems Workshop, Nagoya, Japan, 26–30 January 1997, pp. 25–30.
[5] C.T.-C. Nguyen, Frequency-selective MEMS for miniaturized low-power communication devices, IEEE Trans. Microwave Theory Technol. 47 (8) (1999) 1486–1503.
[6] Y. Oh, B. Lee, S. Baek, H. Kim, J. Kim, S. Kang, C. Song, Surface-micromachined tunable vibratory gyroscope, in: Proceedings of the IEEE International Microelectromechanical Systems Workshop, Nagoya, Japan, 26–30 January 1997, pp. 272–277.

[7] K. Tanaka, Y. Mochida, M. Sugimoto, K. Moriya, T. Hasegawa, K. Atsuchi, K. Ohwada, A micromachined vibrating gyroscope, Sens. Actuators A50 (1995) 111–115.
[8] W.C. Tang, T.-C.H. Nguyen, R.T. Howe, Laterally driven polysilicon resonant microstructures, Sens. Actuators 20 (1989) 25–32.
[9] K. Wang, A.-C. Wong, W.-T. Hsu, C.T.-C. Nguyen, Frequency trimming and *Q*-factor enhancement of micromechanical resonators via localized filament anealing, in: Proceedings of the International Conference on Solid-State Sensors and Actuators (Transducers 97), Chicago, 16–19 June 1997, pp. 109–112.
[10] D. Joachim, L. Lin, Localized deposition of polysilicon for MEMS post-fabrication processing, in: Proceedings of the ASME International Mechanical Engineering Congress and Exposition, Microelectromechanical Systems, Nashville, Tennessee, MEMS, Vol. 1, 1999, pp. 37–42.
[11] K.B. Lee, Y.C. Cho, A triangular electrostatic comb-array for micromechanical resonant frequency tuning, Sens. Actuators A70 (1998) 112–117.
[12] S.G. Adams, F.M. Bertsch, K.A. Shaw, P.G. Hartwell, F.C. Moon, N.C. Macdonald, Capacitance-based tunable resonators, J. Micromech. Microeng. 8 (1998) 15–23.
[13] C. Gui, R. Legtenberg, H. Tilmans, J. Fluitman, M. Elwenspoek, Non-linearity and hysteresis of resonant strain gauges, J. Microelectromech. Syst. 7 (1) (1998) 122–127.
[14] S.G. Adams, F.M. Bertsch, K.A. Shaw, N.C. MacDonald, Independent tuning of linear and non-linear stiffness coefficients, J. Microelectromech. Syst. 7 (2) (1998) 172–180.
[15] J.J. Yao, N.C. MacDonald, A micromachined, single-crystal, silicon, tunable resonator, J. Micromech. Microeng. 6 (1996) 257–264.
[16] R.R.A. Syms, Electrothermal frequency tuning of folded and coupled vibrating micromechanical resonators, J. Microelectromech. Syst. 7 (2) (1998) 164–171.
[17] R.R.A. Syms, D.F. Moore, Focused ion beam tuning of in-plane vibrating micromechanical resonators, Elect. Lett. 35 (1999) 1277–1278.
[18] C. Cabuz, K. Fukatsu, H. Hashimoto, S. Shoji, T. Kurabayashi, K. Minami, M. Esahi, Fine frequency tuning in resonant sensors, in: Proceedings of the IEEE Workshop on Microelectromechanical Systems, Oiso, Japan, 25–28 January 1994, pp. 245–250.
[19] H. Kahn, M.A. Huff, A.H. Heuer, Heating effects on the Young's modulus of films sputtered onto micromachined resonators, Mat. Res. Soc. Proc. 518 (1998) 33–38.
[20] R.I. Pratt, G.C. Johnson, R.T. Howe, J.C. Chang, Mechanical structures for thin film characterization, in: Proceedings of the Digest International Conference on Solid-State Sensors and Actuators (Transducers 91), pp. 205–208.
[21] H. Tilmans, M. Elwenspoek, J. Fluitman, Micro resonant force gauges, Sens. Actuators A30 (1992) 35–53.
[22] MCNC, MEMS Technology Applications Center, Research Triangle Park, NC, 27709.
[23] Canvas, Graphics Software, Deneba Software, Inc., 7400 S.W. 87th Avenue, Miami, FL 33173, USA, 1986.
[24] L. Lin, A.P. Pisano, V.P. Carey, Thermal bubble formations on polysilicon micro resistors, ASME J. Heat Transfer 120 (1998) 735–742.
[25] L. Lin, M. Chiao, Electrothermal response of lineshape microstructures, Sens. Actuators A55 (1996) 35–44.
[26] K.S. Teh, L. Lin, M. Chiao, The creep behaviour of polysilicon microstructure, in: Proceedings of the 10th International Conference on Solid State Sensors and Actuators, Technical Digest (Transducers 99), Sendai, Japan, June 1999, pp. 508–511.